Electronic Supporting Information for:

Vibrational solvatochromism of rhodium pybox carbonyl complexes mediated by hydrogen bonding

Nil Roig,[a,b] Mercedes Alonso,[b,*] and Adrian B. Chaplin[a,*]

[a] *Department of Chemistry, University of Warwick, Gibbet Hill Road, Coventry CV4 7AL, UK.*
Email: a.b.chaplin@warwick.ac.uk

[b] *Eenheid Algemene Chemie (ALGC), Vrije Universiteit Brussel (VUB), 1050 Brussels, Belgium.*
Email: mercedes.alonso@vub.be

Table of contents

1. General considerations

All manipulations were performed under an atmosphere of argon using Schlenk and glove box techniques unless otherwise stated. Glassware was oven-dried at 150 ºC overnight and flame-dried under vacuum prior to use. Molecular sieves were activated by heating at 300 ºC in vacuo overnight. CD_2Cl_2 was freeze-pump-thaw degassed and dried over activated 3 Å molecular sieves. Anhydrous CH_2Cl_2 and hexane were purchased from Acros Organics or Sigma-Aldrich, freeze-pump-thaw degassed and stored over activated 3 Å molecular sieves. [Rh((*R*,*R*)-Ph-pybox)(CO)][BAr^F_4] **1**,[1] and [Rh((*R*,*R*)-Ph-pybox)Cl_2(CO)][BAr^F_4] **2**,[1] dimethyl-pybox,[2] Na[BAr^F_4],[3] and $PhICl_2$[4] were synthesised according to published procedures. $[Rh(CO)_2Cl]_2$ was purchased from Sigma-Aldrich and stored under argon. Carbon monoxide was used from commercial supplier without further purification. NMR spectra were recorded on Bruker spectrometers under argon at 298 K. Chemical shifts are quoted in ppm and coupling constants in Hz. Liquid-phase solution FT-IR measurements were conducted in an Omni-Cell demountable transmission cell by Specac equipped with KBr windows and recorded in a JASCO FT/IR-4200 spectrometer. The samples (3.5 µmol) were sealed in a screw cap vial inside an argon-filled glovebox, opened to air and then immediately dissolved in analytical grade solvent mixtures (1 mL, 3.5 mM) and measured within 30 s. High resolution (HR) ESI-MS were recorded on Bruker Maxis Plus instrument and microanalyses were performed in duplicate at Elemental Microanalysis Ltd.

2. FT-IR spectra of 1 and 2

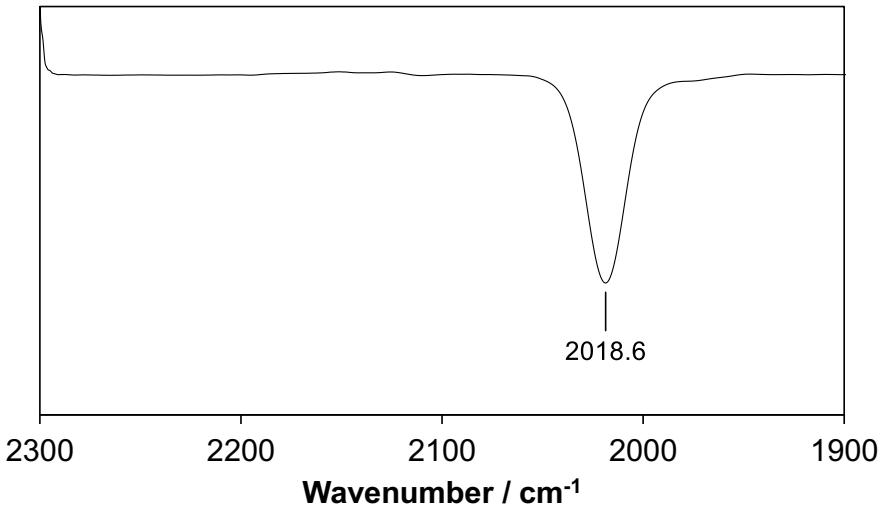

Figure S1. FT-IR spectrum of **1** in dichloromethane.

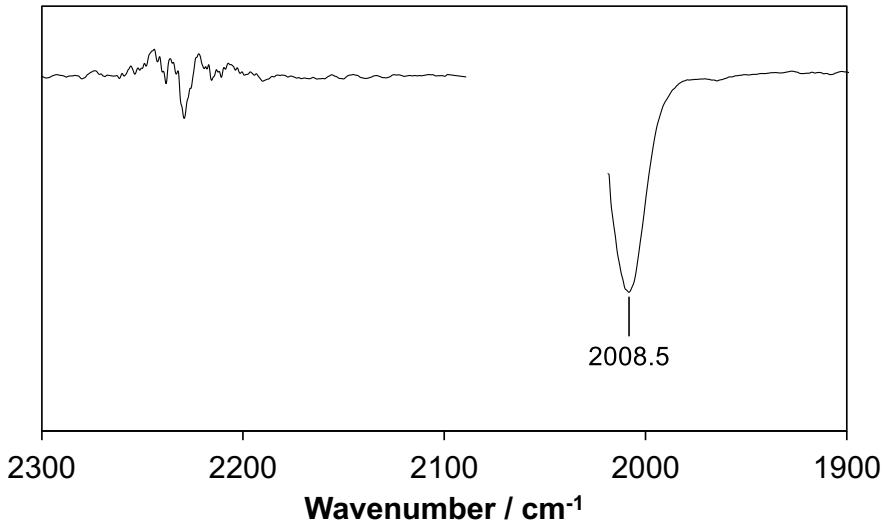

Figure S2. FT-IR spectrum of **1** in methanol. Region between 2018 and 2086 cm^{-1} removed due to saturation from the solvent.

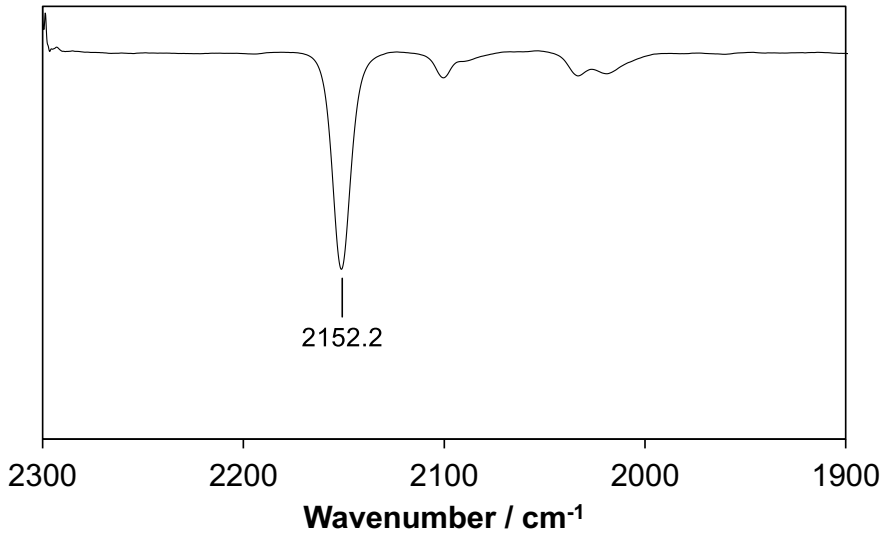

Figure S3. FT-IR spectrum of **2** in dichloromethane.

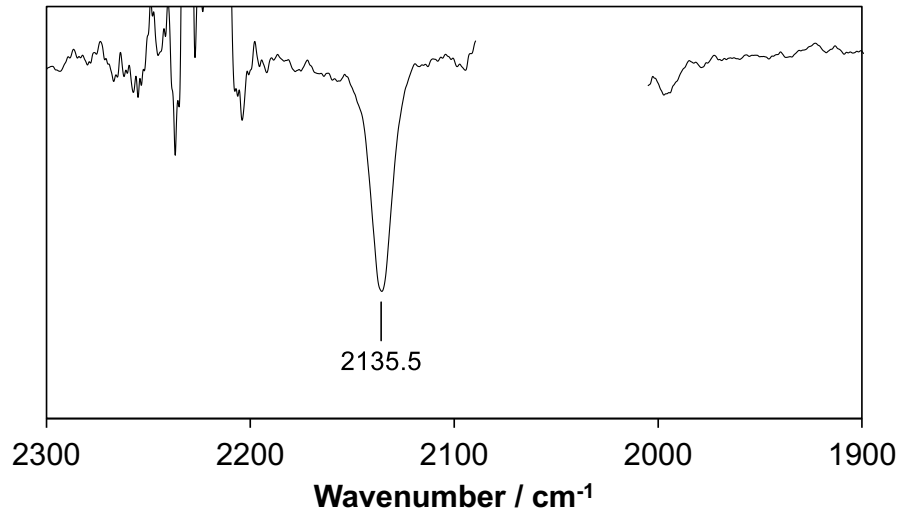

Figure S4. FT-IR spectrum of **2** in methanol. Region between 2005 and 2090 cm^{-1} removed due to saturation from the solvent.

3. Preparation of [Rh(dimethyl-pybox)(CO)][BAr^F_4] 3

A suspension of dimethyl-pybox (3.7 mg, 0.014 mmol), $[Rh(CO)_2Cl]_2$ (2.6 mg, 0.007 mmol) and Na[BAr^F_4] in dichloromethane (0.5 mL) was stirred at room temperature for 30 min. The solution was filtered into a recrystallisation tube and layered with hexane to afford the product as blue/purple crystals on diffusion, some of which were suitable for X-ray diffraction. Yield: 12.9 mg, (0.010 mmol, 75%).

^{1}H NMR (500 MHz, CD_2Cl_2): δ 8.11 (t, $^3J_{HH}$ = 8.0, 1H, py), 7.79 (d, $^3J_{HH}$ = 8.0, 2H, py), 7.70–7.74 (m, 8H, Ar^F), 7.56 (br, 4H, Ar^F), 4.68 (s, 4H, CH_2), 1.40 (s, 12H, CH_3).

^{13}C{^{1}H} NMR (126 MHz, CD_2Cl_2): δ 191.1 (d, $^1J_{RhC}$ = 75, RhCO), 165.8 (s, ox{OCN}), 162.2 (q, $^1J_{CB}$ = 50, Ar^F), 146.9 (s, py), 143.4 (s, py), 135.2 (s, Ar^F), 129.3 (qq, $^2J_{FC}$ = 32, $^3J_{CB}$ = 3, Ar^F), 125.0 (s, py), 125.0 (q, $^1J_{FC}$ = 272, Ar^F), 117.9, (sept, $^3J_{FC}$ = 4, Ar^F), 83.2 (s, CH_2), 67.6 (d, $^3J_{RhC}$ = 2, ox{CMe_2}), 27.7 (s, CH_3).

IR: ν(CO) 2006.6 cm^{-1} (CH_2Cl_2), 1994.3 cm^{-1} (CH_3OH).

HR ESI-MS (MeOH, 180 ºC, 4 kV) positive ion: 404.0482 ($[M]^+$, calcd. 404.0476) *m*/*z*.

Anal. calcd. for $C_{48}H_{31}BF_{24}N_3O_3Rh$ (1267.4712 g·mol^{-1}): C, 45.49; H, 2.47; N, 3.32; found C, 45.37, H, 2.40, N, 3.18.

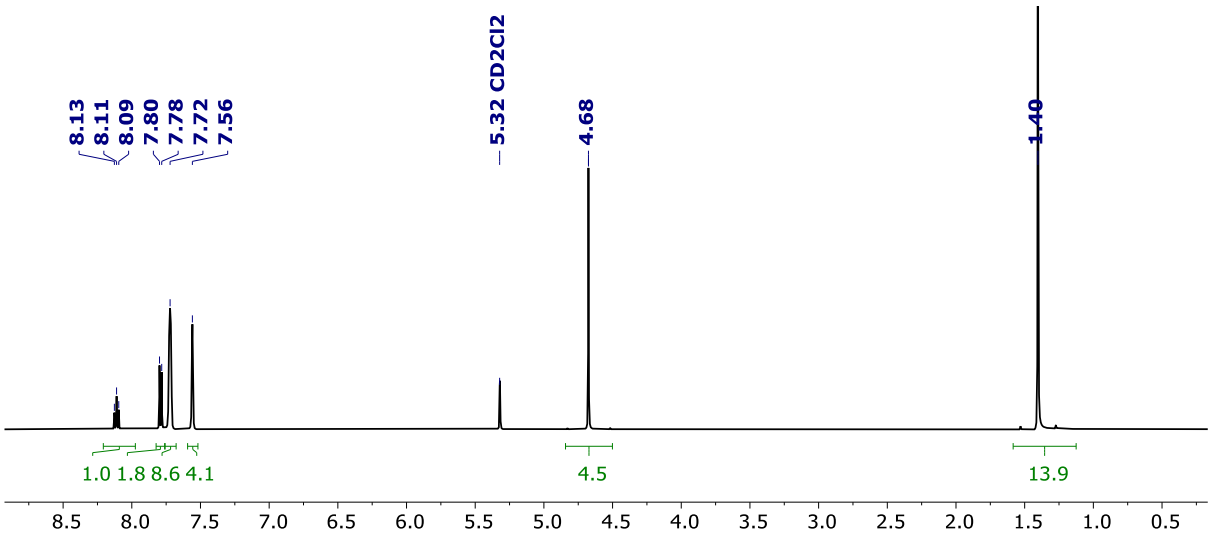

Figure S5. ^{1}H NMR spectrum of **3** in CD_2Cl_2 (500 MHz).

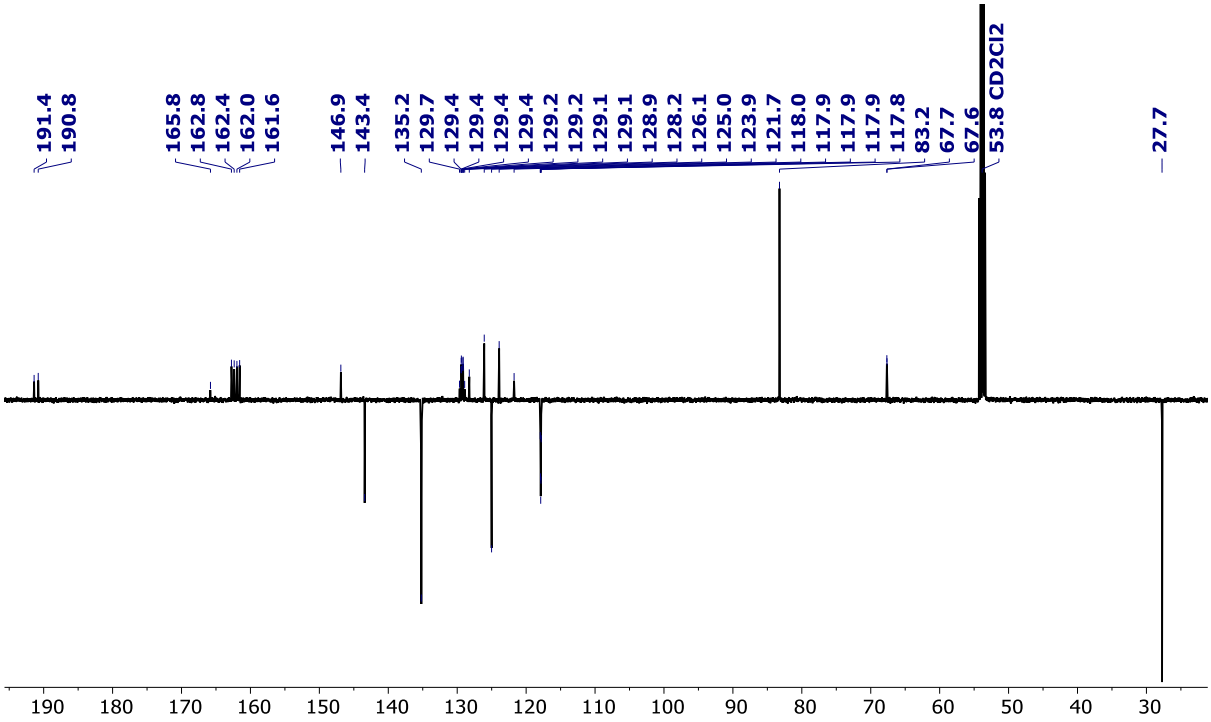

Figure S6. $^{13}C\{^{1}H\}$ NMR spectrum of **3** in CD_2Cl_2 (126 MHz).

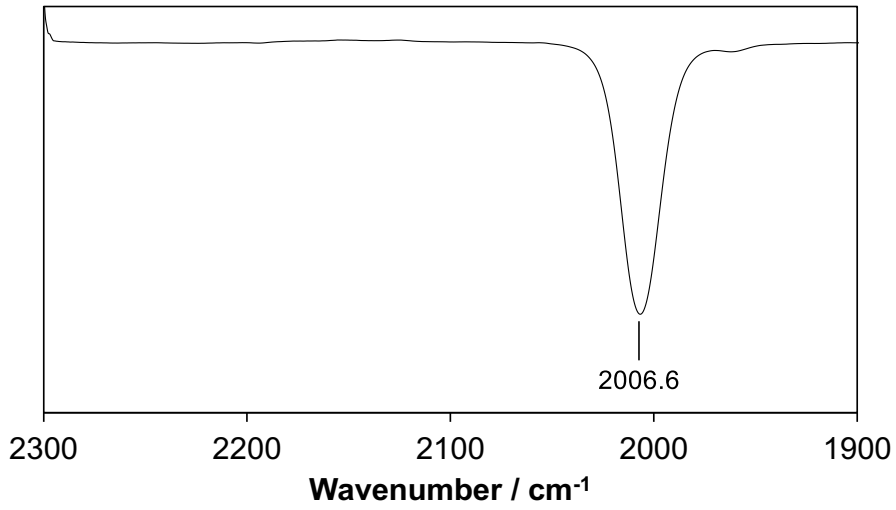

Figure S7. FT-IR spectrum of **3** in dichloromethane.

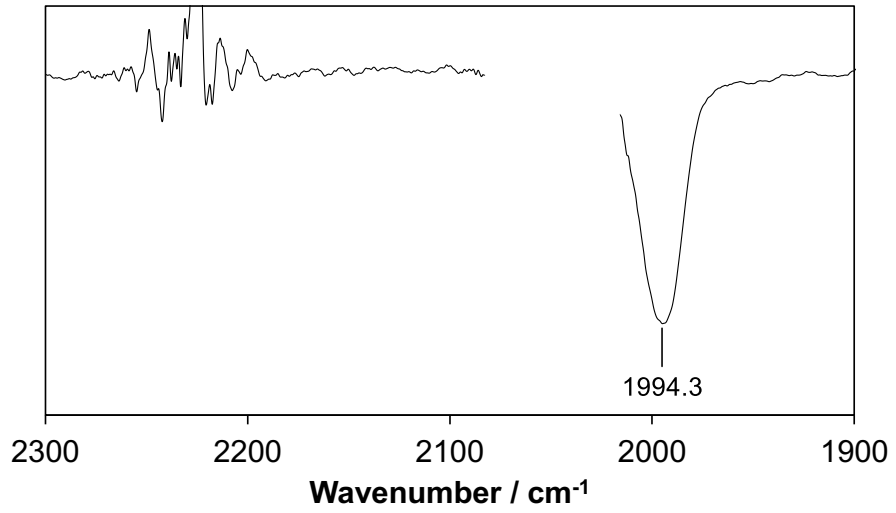

Figure S8. FT-IR spectrum of **3** in methanol. Region between 2016 and 2084 cm^{-1} removed due to saturation from the solvent.

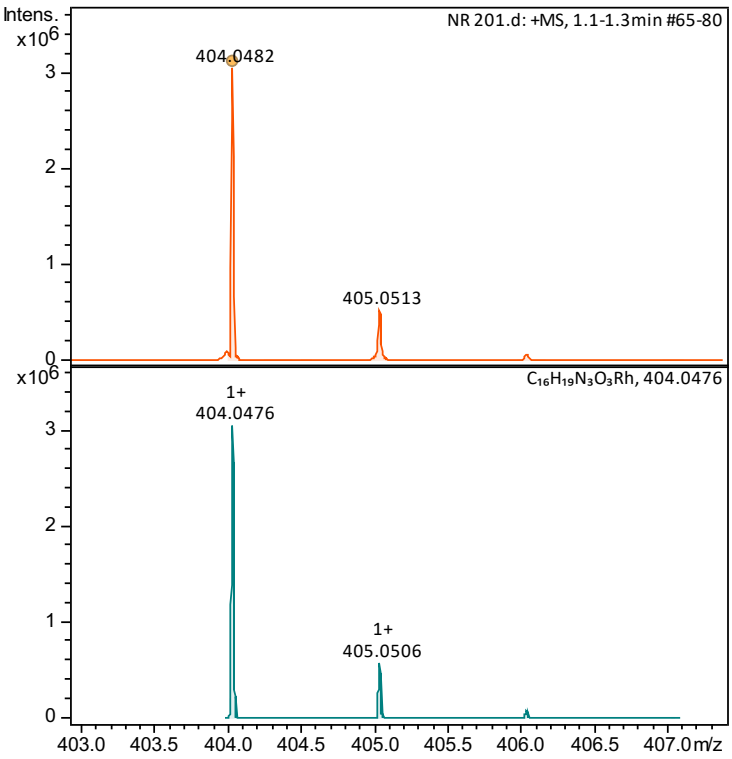

Figure S9. HR ESI-MS of **3**.

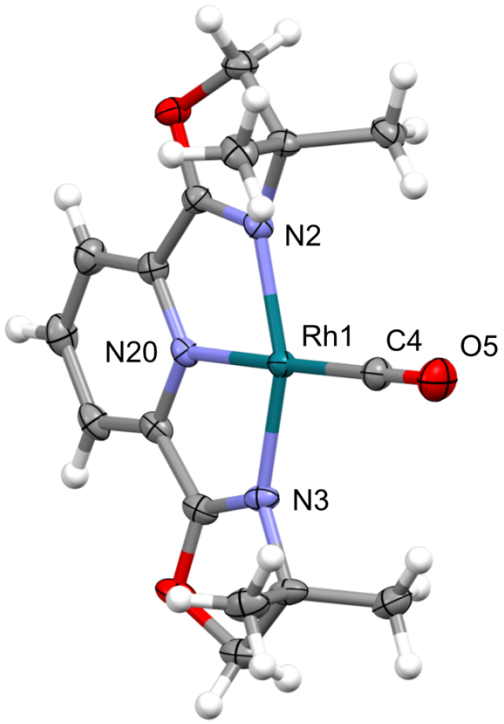

Figure S10. Solid-state structure of **3** (CCDC 2545198). Thermal ellipsoids drawn at 50% probability; anion omitted. Selected bond lengths (Å) and angles (°): Rh1–N2, 2.045(2); Rh1–N3, 2.047(2); Rh1–N20, 2.015(2); Rh1–C4, 1.854(2); C4–O5, 1.131(3); N2–Rh1–N3, 155.82(8); N20–Rh1–C4, 176.1(1).

4. Preparation of [Rh(dimethyl-pybox)Cl_2(CO)][BAr^F_4] 4

A solution of [Rh(dimethyl-pybox)(CO)][BAr^F_4] **3** (250.0 mg, 0.197 mmol) and $PhICl_2$ (54.3 mg, 0.197 mmol) in dichloromethane (10 mL) was stirred at room temperature for 30 min. The solution was filtered into a recrystallisation tube and layered with hexane to afford the product as yellow crystals on diffusion, some of which were suitable for X-ray diffraction. Yield: 209.7 mg (0.157 mmol, 80%).

^{1}H NMR (500 MHz, CD_2Cl_2): δ 8.60 (t $^3J_{HH}$ = 8.0, 1H, py), 8.30 (d, $^3J_{HH}$ = 8.0, 2H, py), 7.70–7.74 (m, 8H, Ar^F), 7.56 (br, 4H, Ar^F), 4.89 (s, 4H, CH_2), 1.63 (s, 12H, CH_3).

^{13}C{^{1}H} NMR (126 MHz, CD_2Cl_2): δ 175.8 (d, $^1J_{RhC}$ = 54, RhCO), 166.1 (s, ox{OCN}), 161.7 (q, $^1J_{CB}$ = 50, Ar^F), 145.3 (s, py), 144.6 (s, py), 135.2 (s, Ar^F), 129.3 (qq, $^2J_{FC}$ = 31, $^3J_{CB}$ = 3, Ar^F), 129.3 (s, py), 125.0 (q, $^1J_{FC}$ = 272, Ar^F), 117.9, (sept, $^3J_{FC}$ = 4, Ar^F), 84.0 (s, CH_2), 69.7 (d, $^3J_{RhC}$ = 1, ox{CMe_2}), 27.9 (s, CH_3).

IR: ν(CO) 2140.8 cm^{-1} (CH_2Cl_2), 2126.9 cm^{-1} (CH_3OH).

HR ESI-MS (MeOH, 180 ºC, 4 kV) positive ion: 473.9862 ([M]$^+$, calcd. 473.9853) *m*/*z*.

Anal. calcd. for $C_{48}H_{31}BCl_2F_{24}N_3O_3Rh$ (1338.3712 g·mol^{-1}): C, 43.08; H, 2.33; N, 3.14; found C, 43.06, H, 2.24, N, 3.04.

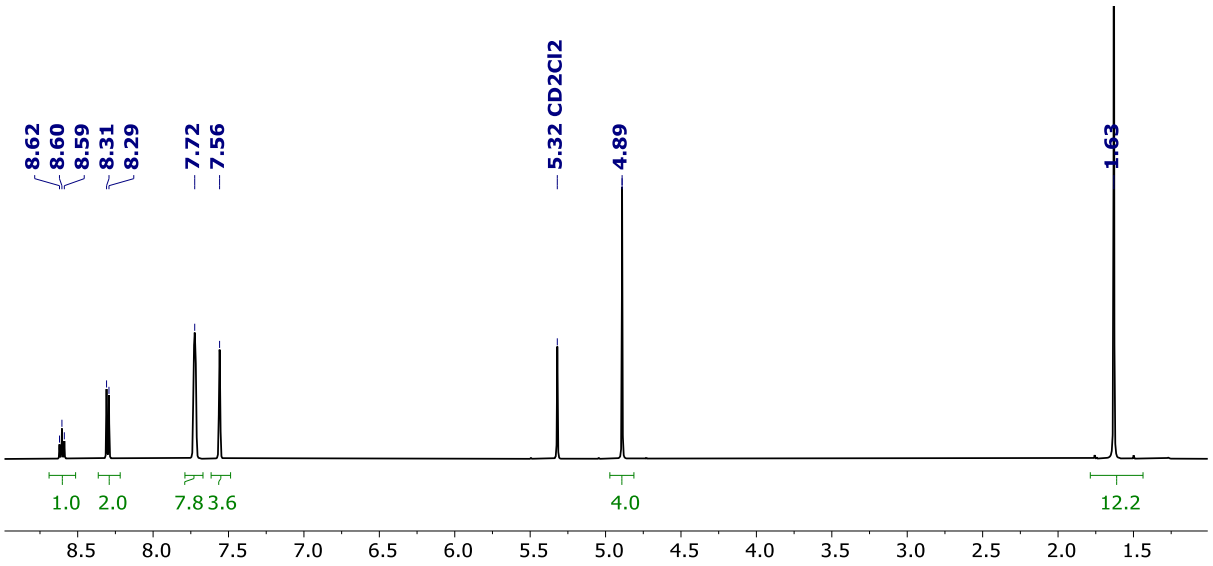

Figure S11. ^{1}H NMR spectrum of **4** in CD_2Cl_2 (500 MHz).

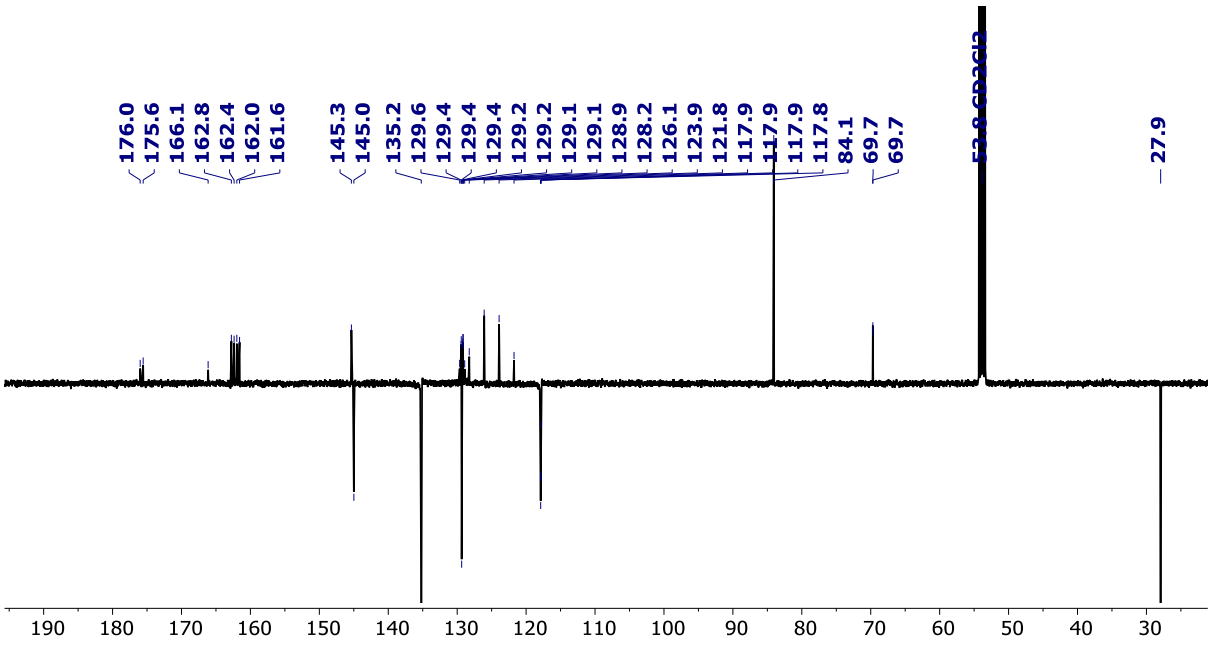

Figure S12. $^{13}C\{^{1}H\}$ NMR spectrum of **4** in CD_2Cl_2 (126 MHz).

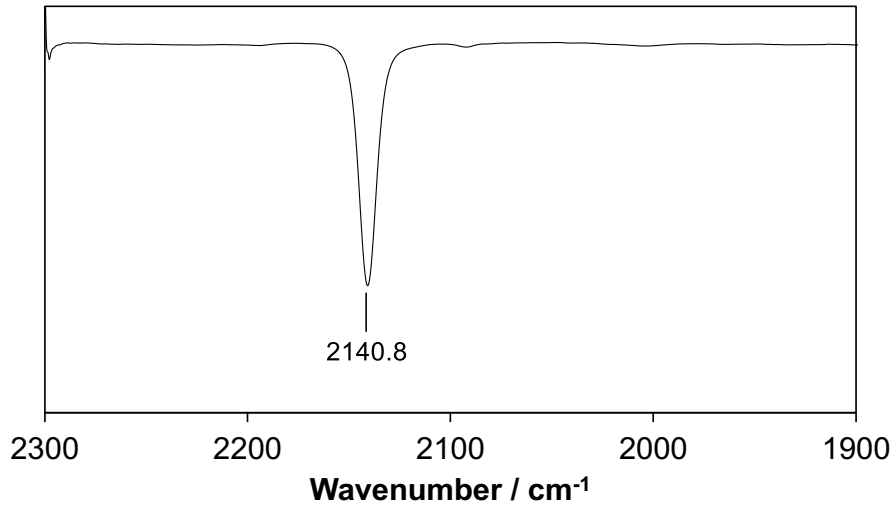

Figure S13. FT-IR spectrum of **4** in dichloromethane.

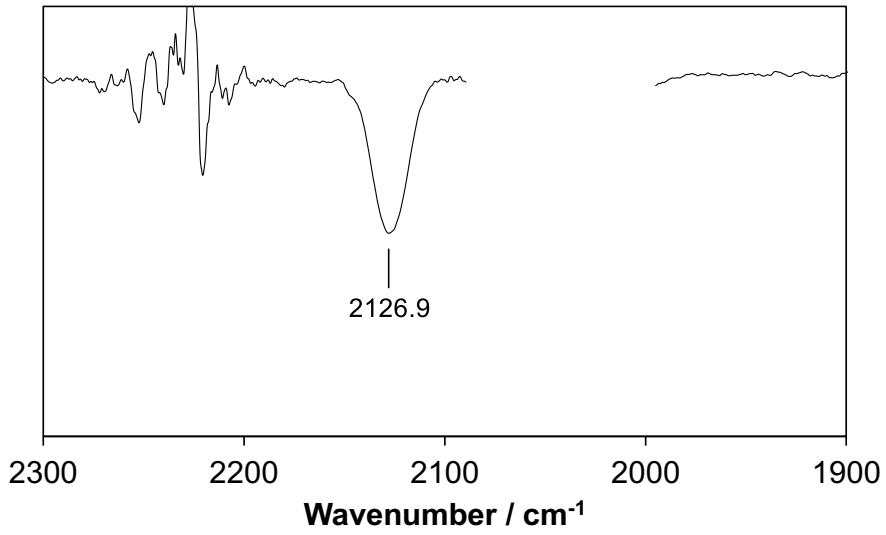

Figure S14. FT-IR spectrum of **4** in methanol. Region between 1990 and 2090 cm^{-1} removed due to saturation from the solvent.

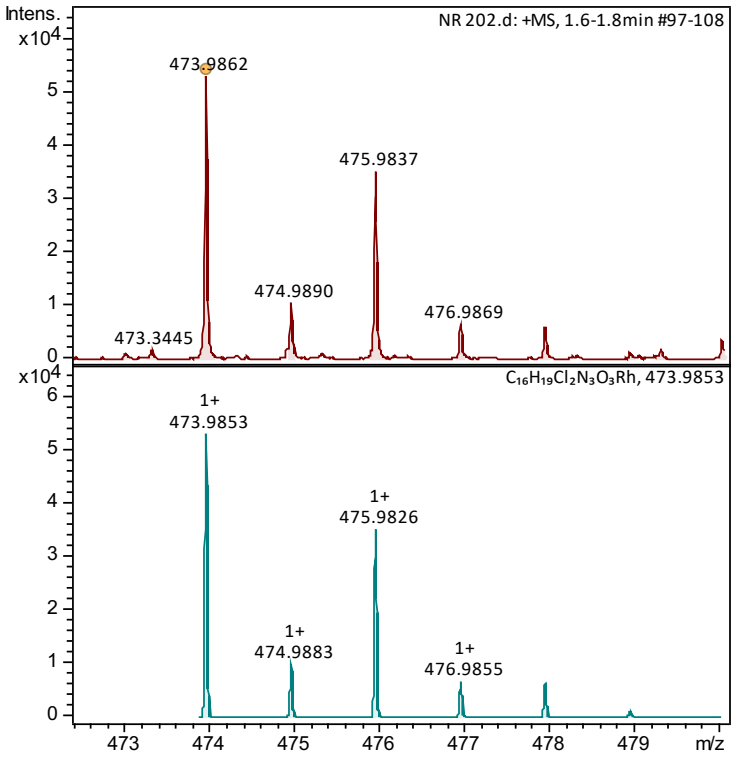

Figure S15. HR ESI-MS of **4**.

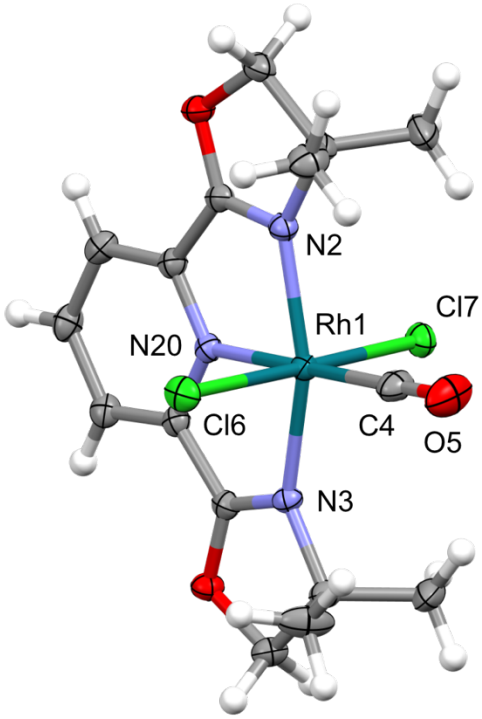

Figure S16. Solid-state structure of **4** (CCDC 2545199). Thermal ellipsoids drawn at 50% probability; anion omitted. Selected bond lengths (Å) and angles (°): Rh1–N2, 2.054(1); Rh1–N3, 2.052(1); Rh1–N20, 1.938(1); Rh1–C4, 1.916(2); Rh1–Cl6, 2.3238(5); Rh1–Cl7, 2.3350(5); C4–O5, 1.122(2); N2–Rh1–N3, 158.04(6); N20–Rh1–C4, 178.61(7); Cl6–Rh1–Cl7, 176.97(2).

5. Values of *ν*(CO) measured in binary mixtures of dichloromethane and methanol

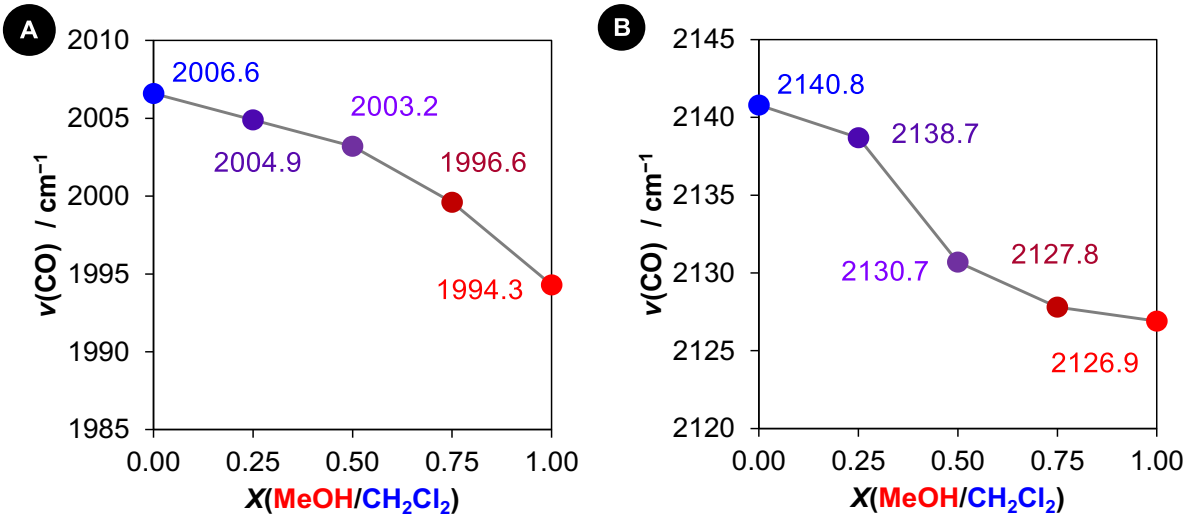

Figure S17. Solvatochromic plots for *ν*(CO) of **3** (A) and **4** (B) in binary mixtures of dichloromethane/methanol.

Table S1. Experimentally determined values of *v*(CO) for **1**, **2**, **3** and **4** in binary mixtures of dichloromethane/methanol (cm^{-1}); Δv(CO) is the shift in methanol relative to dichloromethane.

Complex	$X(MeOH/CH_2Cl_2)$					Δv(CO)
	0.00	**0.25**	**0.50**	**0.75**	**1.00**	
1	2018.6	2017.2	2015.5	2013.1	2008.5	-10.1
2	2151.2	2150.0	2141.6	2138.7	2135.5	-15.7
3	2006.6	2004.9	2003.2	1999.6	1994.3	-12.3
4	2140.8	2138.7	2130.7	2127.8	2126.9	-13.9

6. Static DFT calculations

All calculations were performed using the Gaussian 16 software package (revision A.03).[5] Informed by previous work,[6,7] geometry optimisations and analytical vibrational frequency calculations were carried out using the hybrid GGA B3PW91 functional[8] and Pople's 6-31G(d,p) basis set[9] for all atoms except Rh. The Stuttgart-Dresden (SDD) effective core potential was used for Rh to take into account relativistic effects.[10] When indicated, solvent corrections were introduced using the polarizable continuum model (PCM) or the solvent model based on density (SMD) continuum solvation model.[11] The geometric constraints for **1**(HOMe) were selected after inspection of the AIMD trajectories (Figure S20): *r*(RhCO–HOMe) = 3.25 Å, ∠(RhCO–HOMe) = 142.5° (*vide infra*). Values of *v*(CO) at this level of theory have been scaled by a factor of 0.965, based on the experimental (2143.0 cm^{-1}) and calculated (2220.6 cm^{-1}) values of free carbon monoxide.

The spectroscopic shifts predicted for **1**·HOMe and **1**(HOMe) at the B3PW91/6-31G(d,p) (SDD for Rh) level of theory are substantiated by analysis of **1**, **1**·HOMe and **1**(HOMe) at the B3PW91/6-31++G(d,p) (SDD for Rh), B3PW91-D3BJ/6-31G(d,p) (SDD for Rh) and ωB97X-D/6-31G(d,p) (SDD for Rh) levels of theory (Table S2).[12,13] Values of *v*(CO) for these calculations were scaled using free carbon monoxide as described above.

Table S2. Calculated *v*(CO) values for **1** and **2** (cm^{-1})

System	Conditions	*r*(XH) / Å	*v*(CO)	Δ*v*(CO)
B3PW91/6-31G(d,p) (SDD for Rh)				
1	gas-phase	-	2056.6	-
1	SMD, methanol	-	1961.2	–36.8[a]
1	PCM, methanol	-	1997.2	–10.2[a]
1	SMD, dichloromethane	-	1998.0	-
1	PCM, dichloromethane	-	2007.4	-
1·HOMe	gas-phase	2.52 (X = Rh)	2058.7	+2.0[b]
1(HOMe) constrained	gas-phase	3.25 (X = CO)	2050.1	–6.5[b]
1(HOMe) optimised	gas-phase	2.72 (X = CO)	2038.1	–18.5[b]
2	gas-phase	-	2117.5	-
2	SMD, methanol	-	2127.0	–9.1[a]
2	PCM, methanol	-	2126.7	–4.1[a]
2	SMD, dichloromethane	-	2131.1	-
2	PCM, dichloromethane	-	2117.5	-
B3PW91/6-31++G(d,p) (SDD for Rh)				
1	gas-phase	-	1944.3	-
1·HOMe	gas-phase	2.47 (X = Rh)	1946.6	+2.3[b]
1(HOMe) constrained	gas-phase	3.25 (X = CO)	1940.9	–3.4[b]
1(HOMe) optimised	gas-phase	2.42 (X = CO)	1919.1	–25.2[b]
B3PW91-D3BJ/6-31G(d,p) (SDD for Rh)				
1	gas-phase	-	2064.6	-
1·HOMe	gas-phase	2.32 (X = Rh)	2067.2	+2.5[b]
1(HOMe) constrained	gas-phase	3.25 (X = CO)	2054.7	–10.0[b]
1(HOMe) optimised	gas-phase	2.58 (X = CO)	2040.2	–24.5[b]
ωB97X-D/6-31G(d,p) (SDD for Rh)				
1	gas-phase	-	2073.5	-
1·HOMe	gas-phase	2.50 (X = Rh)	2074.5	+1.0[b]
1(HOMe) constrained	gas-phase	3.25 (X = CO)	2062.1	–11.4[b]
1(HOMe) optimised	gas-phase	2.64 (X = CO)	2051.5	–22.0[b]

[a] Relative to *v*(CO) for **1**/**2** in dichloromethane; [b] Relative to *v*(CO) for **1** in the gas-phase.

7. External electric field calculations

Complexes **1** and **2** were optimised under the influence of oriented external electric fields (OEEFs) of varying magnitude along the C–O axis at the B3PW91/6-31G(d,p) (SDD for Rh) level of theory. Consistent with previous results,[7,14] positive fields induce an increase of *v*(CO) and vice versa. These calculations indicate that rhodium(I) complex **1** is more susceptible to polarization effects than **2**, as quantified by the larger gradients in Figure S18 and consistent with the implicit solvation calculations.

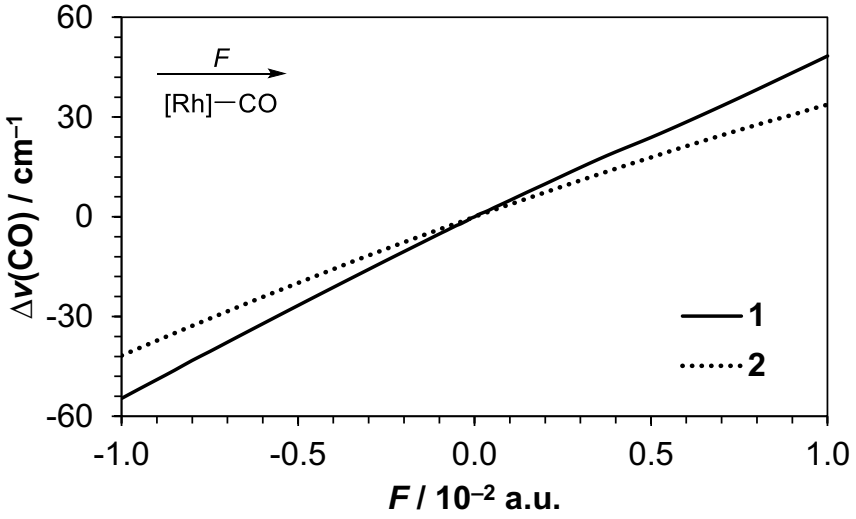

Figure S18. Effect of an external electric field applied along the M→CO vector on the values of ν(CO) for **1** and **2**. 1 a.u. = 5.14 × 10^3 MV·cm^{-1}.

8. Explicit solvation via AIMD simulations of 1 and 2

Simulations were conducted using the open-source CP2K software (Version 6.1) with the Quickstep implementation.[15] Forces driving the simulations were calculated "on the fly" using the PBE GGA functional[16] including Grimme's D3 long-range dispersion corrections[13] and the DZVP-MOLOPT-GTH (DZVP-MOLOPT-SR-GTH for Rh)[17] plane wave basis set with the grid level cut-off set at 250 Ry and the relative cut-off set at 80 Ry. The production runs (20,000 steps with a timestep of 0.5 fs) were preceded by an equilibration phase of 5,000 steps with a timestep of 0.5 fs. Simulations were performed in an NVT ensemble with the temperature set at 298 K and controlled by the CSVR thermostat[18] using a time constant of 1 fs during the equilibration phase and 50 fs during the production runs. Dichloromethane and methanol were optimised with Gaussian 16 at the B3PW91/6-31G(d,p) level of theory, and the resulting geometries, along with those of **1** and **2,** were employed to construct a solvated cubic box using the Packmol software (version 20).[19] The cube edge was set to 18 Å, and 43 and 66 molecules of dichloromethane (1.33 g·mL^{-1}) and methanol (0.79 g·mL^{-1}) were added, respectively based on the following equation:

$$n_{solvent} = (V_{box} - V_{solute}) \cdot \frac{\rho_{solvent} \cdot N_A}{MW_{solvent}}$$

Where $n_{solvent}$ is the optimal number of solvent molecules, V_{box} is the volume of the periodic box, V_{solute} is the volume of a sphere of diameter 13 Å (based on the longest interatomic distance in the optimised structures of **1** and **2** (~11 Å) plus 1 Å to account for padding between solute and solvent), $\rho_{solvent}$ is the density of the solvent, N_A is Avogadro's number and $MW_{solvent}$ is the molar weight of the solvent. During the simulations, Wannier centres were localised for every 5 steps across the final 10,000 steps of the production run.[20] Analysis of these data using the Travis analyser software[21] resulted in the simulated IR spectra and ν(CO) values.

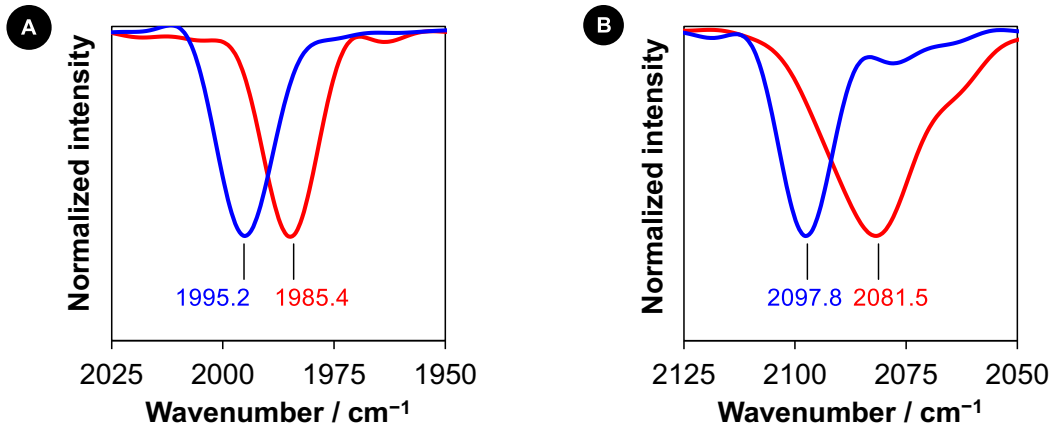

Figure S19. Simulated IR spectra of **1** (A) and **2** (B) in the presence of explicit dichloromethane (blue) and methanol (red). Intensities have been normalised to the *v*(CO) maximum.

Statistical analysis of selected geometrical parameters from the trajectories is provided in Table S3. The formation of the Rh···HOMe adduct in the **1**/MeOH simulations (cf. Figure 2A) is indirectly evidenced by a reduction in the average dihedral angle for one of the flanking oxazoline rings relative to the other (*viz.* -110 vs. 129°). These torsions are effectively equivalent in all the other simulations. The maxima observed in the distribution plot of *r*(RhCO–HOMe) and ∠(RhCO–HOMe) for **1**/MeOH (Figure S20) informed the constraints used in the static DFT analysis of **1**(HOMe).

Table S3. Geometric parameters for AIMD simulations of **1** and **2**[a]

Parameter	**1**/CH_2Cl_2	**1**/MeOH	**2**/CH_2Cl_2	**2**/MeOH
|C≡O| / Å	1.162(14)	1.162(10)	1.146(10)	1.148(19)
|Rh–C| / Å	1.854(39)	1.851(33)	1.895(35)	1.893(37)
$\|\angle N_{py}–Rh–C\|$ / °	168(7)	173(4)	174(3)	174(3)
$\|\angle O–C–C–C_{Ph}\|$ / °	-121(17)	-129(12)	-133(12)	-134(14)
$\|\angle O–C–C–C_{Ph}\|$ / °	-127(18)	-110(17)	-132(13)	-135(12)
v(CO) / cm^{-1}	1995.2	1985.4	2097.8	2081.5

[a] Averaged over the full 20,000 steps, except for the simulated values of *v*(CO) which were determined over the last 10,000 steps. Standard deviations in parenthesis.

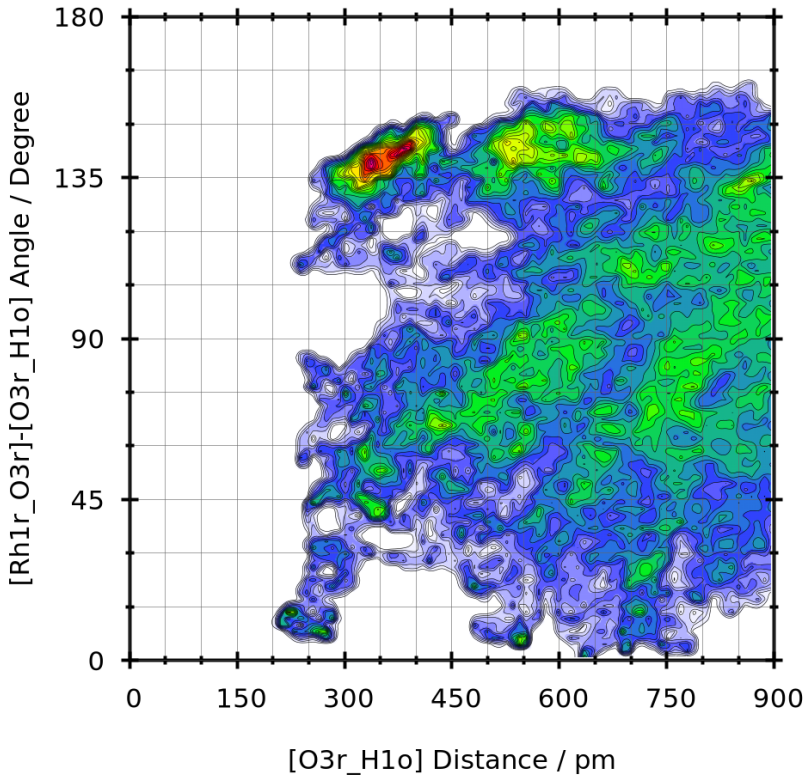

Figure S20. Distribution plot for the *r*(RhCO–HOMe) distances and ∠(RhCO–HOMe) angles observed during the **1**/MeOH simulation.

9. References

1 G. L. Parker, S. Lau, B. Leforestier and A. B. Chaplin, *Eur. J. Inorg. Chem.*, 2019, 3791–3798.

2 Y.-Y. Zhu, C.-W. Liu, J. Yin, Z.-S. Meng, Q. Yang, J. Wang, T. Liu and S. Gao, *Dalton Trans.*, 2015, **44**, 20906–20912.

3 W. E. Buschmann, J. S. Miller, K. Bowman-James and C. N. Miller, *Inorg. Synth.*, 2002, **33**, 83–91; A. J. Martínez-Martínez and A. S. Weller, *Dalton Trans.*, 2019, **48**, 3551–3554.

4 J. Yu and C. Zhang, *Synthesis*, 2009, 2324–2328.

5 Gaussian 16, Revision A.03, M. J. Frisch, G. W. Trucks, H. B. Schlegel, G. E. Scuseria, M. A. Robb, J. R. Cheeseman, G. Scalmani, V. Barone, G. A. Petersson, H. Nakatsuji, X. Li, M. Caricato, A. V. Marenich, J. Bloino, B. G. Janesko, R. Gomperts, B. Mennucci, H. P. Hratchian, J. V. Ortiz, A. F. Izmaylov, J. L. Sonnenberg, D. Williams-Young, F. Ding, F. Lipparini, F. Egidi, J. Goings, B. Peng, A. Petrone, T. Henderson, D. Ranasinghe, V. G. Zakrzewski, J. Gao, N. Rega, G. Zheng, W. Liang, M. Hada, M. Ehara, K. Toyota, R. Fukuda, J. Hasegawa, M. Ishida, T. Nakajima, Y. Honda, O. Kitao, H. Nakai, T. Vreven, K. Throssell, J. A. Montgomery Jr., J. E. Peralta, F. Ogliaro, M. J. Bearpark, J. J. Heyd, E. N. Brothers, K. N. Kudin, V. N. Staroverov, T. A. Keith, R. Kobayashi, J. Normand, K. Raghavachari, A. P. Rendell, J. C. Burant, S. S. Iyengar,

J. Tomasi, M. Cossi, J. M. Millam, M. Klene, C. Adamo, R. Cammi, J. W. Ochterski, R. L. Martin, K. Morokuma, O. Farkas, J. B. Foresman and D. J. Fox, Gaussian, Inc., Wallingford, CT, 2016.

6 G. L. Parker, R. V. Lommel, N. Roig, M. Alonso and A. B. Chaplin, *Chem. A Eur. J.*, 2022, **28**, e202202283.

7 N. Roig, R. V. Lommel, M. Alonso and A. B. Chaplin, *Organometallics*, 2024, **43**, 2787–2796.

8 A. D. Becke, *Phys. Rev. A*, 1988, **38**, 3098–3100; A. D. Becke, *J. Chem. Phys.*, 1993, **98**, 5648–5652.

9 R. Ditchfield, W. J. Hehre and J. A. Pople, *J. Chem. Phys.*, 1971, **54**, 724–728.

10 D. Andrae, U. Häußermann, M. Dolg, H. Stoll and H. Preuß, *Theor. Chim. Acta*, 1990, **77**, 123–141; A. W. Ehlers, M. Böhme, S. Dapprich, A. Gobbi, A. Höllwarth, V. Jonas, K. F. Köhler, R. Stegmann, A. Veldkamp and G. Frenking, *Chem. Phys. Lett.*, 1993, **208**, 111–114.

11 S. Miertuš, E. Scrocco and J. Tomasi, *Chem. Phys.*, 1981, **55**, 117–129; J. Tomasi, B. Mennucci, R. Cammi, *Chem. Rev.*, 2005, **105**, 2999–3094; A. V. Marenich, C. J. Cramer and D. G. Truhlar, *J. Phys. Chem. B*, 2009, **113**, 6378–6396.

12 T. Clark, J. Chandrasekhar, G. W. Spitznagel and P. Von Ragué Schleyer, *J. Comput. Chem.* 1983, **4**, 294–301; S. Grimme, S. Ehrlich and L. Goerigk, *J. Comput. Chem.*, 2011, **32**, 1456–1465; J.-D. Chai and M. Head-Gordon, *J. Chem. Phys.*, 2008, **128**, 084106.

13 S. Grimme, J. Antony, S. Ehrlich and H. Krieg, *J. Chem. Phys.*, 2010, **132**, 154104.

14 J. L. Andrés, M. Duran, A. Lledós and J. Bertrán, *Chem. Phys.*, 1991, **151**, 37–43; S. Sowlati-Hashjin and C. F. Matta, *J. Chem. Phys.*, 2013, **139**, 144101.

15 J. VandeVondele, M. Krack, F. Mohamed, M. Parrinello, T. Chassaing and J. Hutter, *Comput. Phys. Commun.*, 2005, **167**, 103–128; J. Hutter, M. Iannuzzi, F. Schiffmann and J. VandeVondele, *WIREs Comput. Mol. Sci.*, 2014, **4**, 15–25.

16 J. P. Perdew, K. Burke, M. Ernzerhof, *Phys. Rev. Lett.*, 1996, **77**, 3865–3868.

17 E. van Lenthe and E. J. Baerends, *J. Comput. Chem.*, 2003, **24**, 1142–1156.

18 G. Bussi, D. Donadio and M. Parrinello, *J. Chem. Phys.*, 2007, **126**, 014101.

19 L. Martínez, R. Andrade, E. G. Birgin and J. M. Martínez, *J. Comput. Chem.*, 2009, **30**, 2157–2164.

20 N. Marzari, A. A. Mostofi, J. R. Yates, I. Souza and D. Vanderbilt, *Rev. Mod. Phys.*, 2012, **84**, 1419–1475.

21 M. Brehm, M. Thomas, S. Gehrke and B. Kirchner, *J. Chem. Phys.*, 2020, **152**, 164105.